Online die temperature measurement using S-parameters in GaN-based power converters

Yoann Pascal, Frank Daschner, Stefan Mönch, Marco Liserre, Michael Höft, Rüdiger Quay

Online Die Temperature Measurement Using S-Parameters in GaN-Based Power Converters

Yoann Pascal[a,*], Frank Daschner[b], Stefan Mönch[c], Marco Liserre[a,d], Michael Höft[b], Rüdiger Quay[c]

[a] *Fraunhofer Institute for Silicon Technology ISIT, Fraunhoferstr. 1, 25524 Itzehoe, Germany*
[b] *Chair of Microwave Engineering, Kiel University, Kiel, Germany*
[c] *Fraunhofer Institute for Applied Solid State Physics IAF, Tullastrasse 72, 79108 Freiburg, Germany*
[d] *Chair of Power Electronics, Kiel University, Kiel, Germany*

Abstract

Die temperature (T_j) measurement of GaN HEMTs is of high interest to enable reducing design margin and the implementation of reliability driven control schemes and protections. On-state resistance ($R_{ds,on}$) has been identified as a relevant thermo-electric sensitive parameter (TSEP) for T_j measurement requiring no extra temperature sensor. It is commonly measured in time-domain, based on the on-state voltage drop and the load current. In this work, the T_j of a GaN-on-Si power IC in a dc-dc converter is deduced from measurements conducted online, directly in the frequency domain using RF injection and S-parameter measurements. Thereby, the stimulus is injected on top of the processed power to probe either $R_{ds,on}$, or the resistance of an on-chip Schottky diode used as thermal sensor. Temperature dependent experimental validation up to 150°C is performed on a switching dc-dc power converter, validating the approach for online temperature measurement using RF injection.

1 Introduction

Knowledge of power semiconductors' temperatures is of importance to implement condition monitoring, reliability driven control, thermal protection, dynamic power reserve, design margin reduction, etc [1]. This is gaining further interest when considering wide-bandgap (WBG) devices, which are generally more fragile and have lower thermal capacity than their silicon counterparts [2], [3].

Extensive research work has been dedicated to the online monitoring of dies' temperature. Thermal estimators and observers, including digital twins, have been extensively investigated, but they remain sensitive to the accuracy of the thermal network and power losses modelling [4]. Measurements using thermo-sensitive electrical- or optical- parameters (TSEPs & TSOPs) have also been the focus of extensive research [5]–[7]. In particular, the on-state voltage-drop ($V_{ce,sat}$, $R_{ds,on}$) has been demonstrated to be a valuable TSEP, owing to its sensitivity and relative simplicity of measurement, which has been, so far, performed in time-domain [8], [9].

On-chip sensor integration has also been investigated, but received limited interest from industry, due to the required extra signal conditioning hardware and afferent cost. This approach may nonetheless gain relevance when considering the increasing role played by power electronics in applications that are mission-critical or with high downtime cost. This is further emphasised with GaN devices, the fragility and sensitivity towards parasitics of which strongly increases the relevance of integrating not only the power devices, but also a driver and monitoring functions in power ICs [10].

This paper proposes an approach to measure online the die temperature of GaN power ICs, directly in the frequency domain. Two methods are proposed: through the temperature dependence of the main power transistor on-state resistance ($R_{ds,on}$) on the one hand, and through the dynamic resistance of an on-chip Schottky diode, used as temperature sensor, on the other. Section 2 and 3 describe the devices under study and the test set-up. Experimental results obtained using the on-chip Schottky diode are shown

*Corresponding author: yoann.pascal@isit.fraunhofer.de

This research was partially funded by the Ministry of Education, Science and Culture of the state Schleswig-Holstein (MBWK SH), Germany – project "ISIT@CAU".

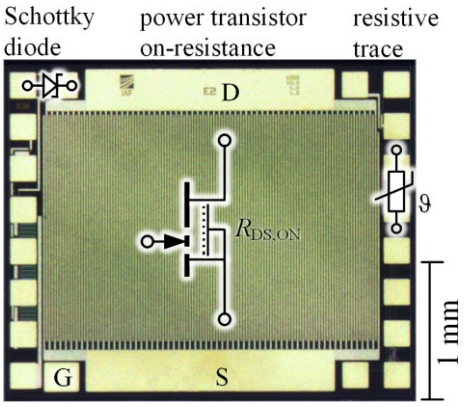

Fig. 1: Chip photo of the 2.5×3 mm² GaN power IC used, showing connections to the mains pads.

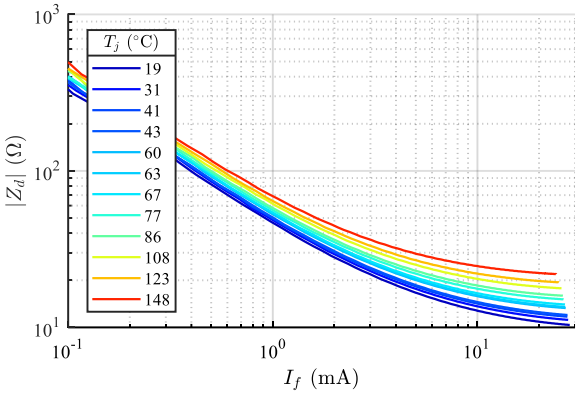

Fig. 2: Dynamic impedance ($Z_d = dv_f/di_f$) of the on-chip GaN Schottky diode vs. current, measured at 1 MHz.

in section 4, and those resulting from the use of the on-state resistance of the transistor are shown in section 5. Section 6 offers a discussion on the approach and results. Finally, section 7 concludes the paper.

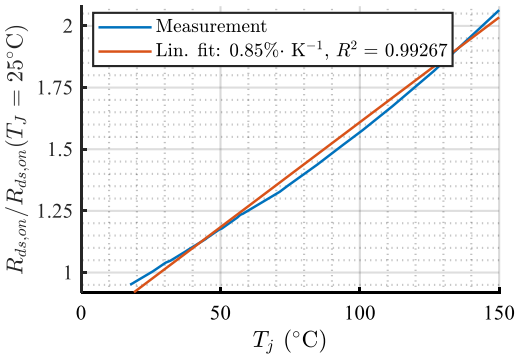

Fig. 3: Normalised HEMT resistance vs. temperature.

2 GaN-on-Si transistors under study

GaN-on-Si power ICs produced by Fraunhofer IAF [11] where used in this study. They integrate on a single 2.5×3 mm² chip (see Fig. 1), amongst other functionality, a power HEMT (600 V-class, 100 mΩ on-resistance, normally-off), a resistive temperature sensor made of thin-film gold metallization [12] wire with typical room-temperature resistance 100 Ω, and a Schottky diode. The thermistor and the GaN diode are isolated from the power transistor.

Fig. 2 shows the measured dynamic resistance of the Schottky diode as a function of temperature. Z_d corresponds to the slope of the forward characteristic of the diode, namely: $Z_d = dv_f/di_f$. At low forward current, the forward voltage is dominated by the junction, hence the decrease in dynamic impedance with the current, and its stabilisation at higher forward current. This impedance exhibits a 2.3 %/K increase temperature coefficient at $I_f = 10$ mA.

Fig. 3 shows the variation of power HEMT $R_{ds,on}$ with temperature.

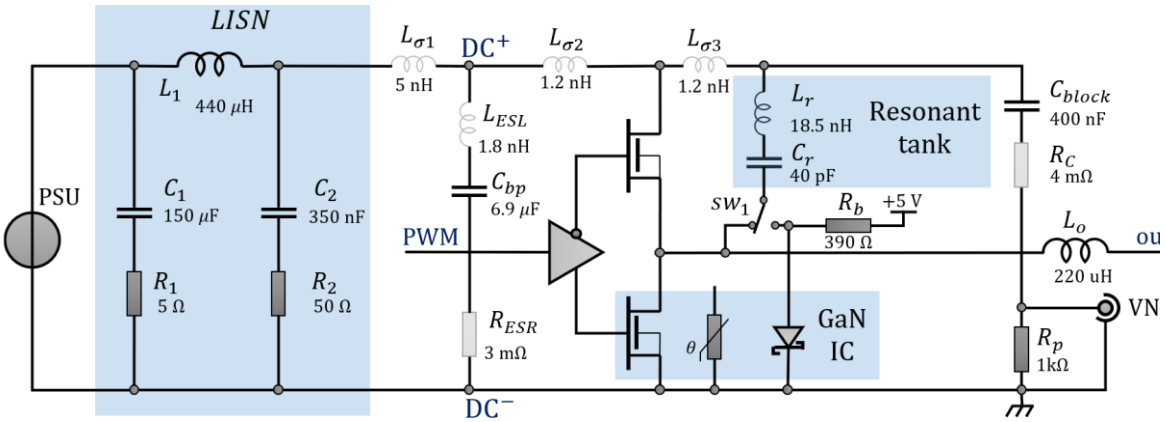

Fig. 4: Simplified schematic of the converter under test. Components in light grey account for some parasitic elements of the circuit, their values were estimated through measurement or simple analytical modelling

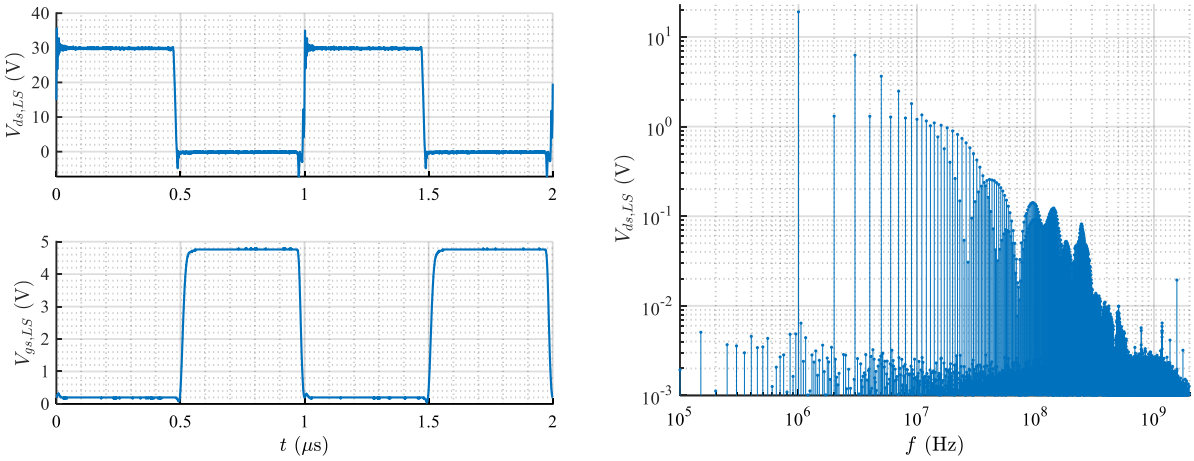

Fig. 5: operation of the converter for a 1 MHz-switching frequency and 50% duty-cycle, under a 30 V-dc-link voltage, and with a 1 A constant load current. Switching node voltage in time- (top left) and frequency (right) domains as well as low-side gate to source voltage (bottom left).

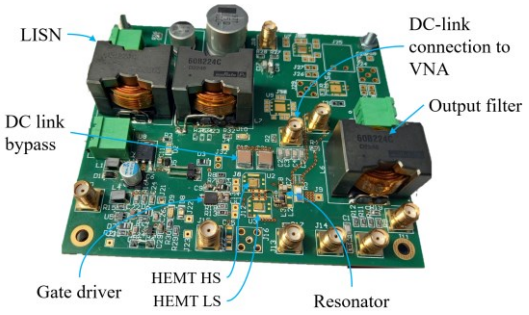

Fig. 6: Annotated photograph of the prototype, highlighting its main elements.

3 Experimental set-up

The schematic of the developed half bridge and a photograph of the prototype are given in Fig. 4 & 6. The GaN ICs constituting the switching cell are directly soldered and wire-bonded on the circuit PCB, using multiple 20 µm AlSi wire bonds and a Kelvin source, without potting. A half bridge driver LM5113 is used, implementing a bootstrap for the high-side switch and additional gate resistances of $R_{g,on}$ =10 Ω & $R_{g,off}$ =0 Ω. Dead-times are 20 ns and 26 ns, with a measured jitter below 400 ps. Ceramic bypass capacitors decouple the switching loop, the parasitic loop inductance of which was minimised for optimal operation [13]. Operation was validated for a 1 MHz-switching frequency, under a 30 V-dc-link voltage, and with a 1 A constant load current (Fig. 5). In these conditions, a single oscillation mode is visible, at 247 MHz [14], with a 16%-voltage overshoot. The power source is connected through a Line Impedance Stabilisation Network (LISN), offering a differential calibrated impedance of 50 Ω ±20% on the DC link, over the measured frequency band 11 kHz – 70 MHz. This is not required by the proposed approach, but ensures a repeatable test environment. The PCB is mounted on a hot plate, allowing to control the temperature of the power devices.

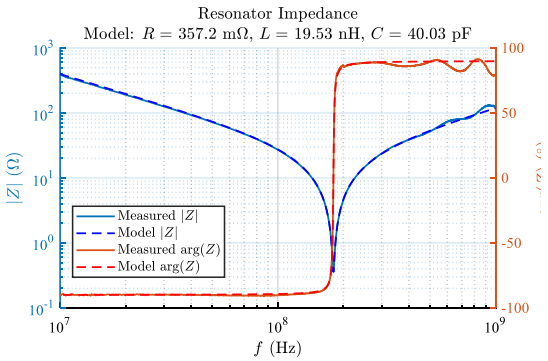

Fig. 7: Measured impedance of the LC circuit used as resonant tank to couple the device used as temperature sensor to the dc link.

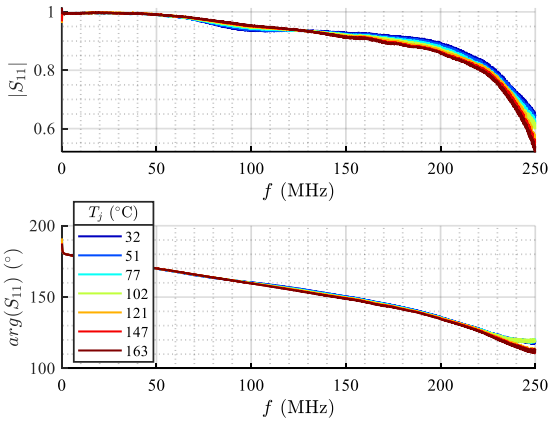

Fig. 8: S_{11} parameter measured for various temperatures, with the diode inserted in the resonant circuit.

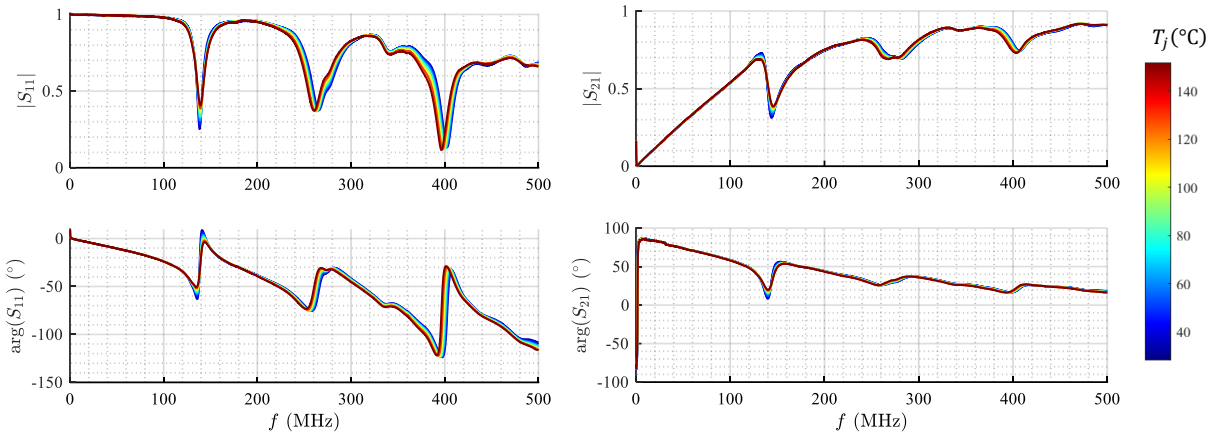

(a) (b)

Fig. 9: S_{11} (a) and S_{21}-shunt (b) parameters measured for various temperatures, with the on-state resistance of the low side (LS) HEMT inserted in the resonant circuit.

In addition, a circuit to measure either the on-state resistance of the low side (LS) transistor or the dynamic resistance of the on-chip Schottky diode is implemented. To this end, the resistance under study is connected in series with a high frequency inductor and capacitor, the resulting RLC-circuit being directly connected across the DC link. The selected inductor is an 18 nH high-Q air-core device from Coilcraft (series 0805HQ-18NXGRB); and 251R15S100JV4E C0G capacitors from Johanson Tech. were used. The impedance of the resulting series LC-circuit, measured in S_{21}.-shunt mode [15] is given in Fig. 7.

A vector network analyser (VNA) is capacitively coupled to the DC link to measure its scattering parameter S_{11}, which is related to the impedance of the dc link, as seen by the instrument.

The Schottky diode is forward biased by a current equal to 10 mA, so as to polarise it in the part of its characteristic where the current has low impact on the dynamic resistance (see Fig. 2), and where the temperature has low impact on the forward voltage.

The resistance of the on-chip resistive temperature sensor, previously calibrated, is measured by a desk bench 4W-ohmmeter to assess the chip temperature. This sensor is solely used in the experiment for temperature monitoring whilst the frequency response including either the $R_{ds,on}$ of the LS power transistor or the Schottky diode is investigated. One of the two sensors ($R_{ds,on}$ or diode) is selected using the switch SW1 in Fig. 4.

A low-end VNA [16] is used for the tests, delivering -10 dBm of power (into 50 Ω) and with full SOLT calibration. The intermediate frequency bandwidth (IFBW) of the instrument is not specified, and the transfer function of the IF filter exhibit a complex shape that depends upon the central frequency.

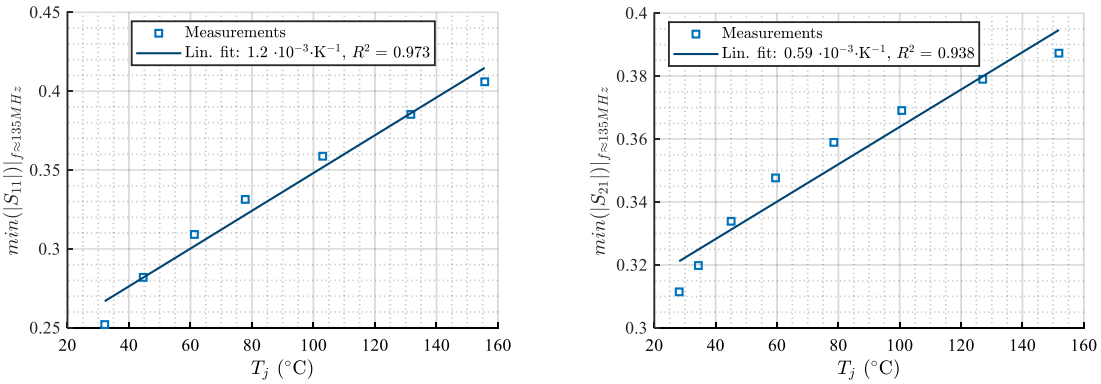

(a) (b)

Fig. 10: Minimum value reached by $|S_{11}|$ (a) and $|S_{21}|$ (b) around 135 MHz, with the on-state resistance of the LS HEMT inserted in the resonant circuit

4 Experimental results – Schottky diode dynamic resistance

A first series of tests was performed by measuring the S_{11}-parameter of the dc link, with the Schottky diode connected across the dc link through the resonant circuit. The converter was supplied with a 30 V dc link voltage, was operated at 100 kHz and 50%-duty cycle, and supplied a 15 Ω load through a $L_o = 220$ µH inductance (self-resonant frequency: 33 MHz) leading to a 1 A output current. Fig. 8 shows the results of the S_{11} measurements as a function of frequency, for various temperatures of the LS chip (assessed using the embedded resistive sensor).

A light, though clear shift of the scattering parameters can be observed, which could be used for temperature extraction. Nonetheless, the high dynamic resistance of the diode (~10 Ω – see Fig. 2) limits the sensitivity, due to its parallel connection to the low-impedance dc link capacitor.

5 Experimental results – GaN *HEMT* on-state resistance $R_{ds,on}$

Measurements were conducted with the resonant tank connected between the DC+ and the midpoint of the switching cell. Two series of test were performed, the first in static operation, with the LS-transistor constantly in the on-state, and the other under switching conditions. The S_{11}-parameter of the dc link therefore exhibited a dependence in temperature, due to that of the $R_{ds,on}$ of the LS transistor during its on-time, which constitute a significant share of the damping at the tank's resonant frequency.

5.1 Static operation

S_{11} Measurements

The converter was supplied with a 30 V dc link voltage, but to avoid the need for synchronising the VNA and the PWM signal, the LS device remained constantly turned on in the tests reported in this sub-section. A 30 Ω – 220 µH load was connected in between the DC+ and the output.

The spectral response with temperature as parameter, given in Fig. 9-a, shows a clear dependence of $|S_{11}|$ with temperature, in particular around the resonator's central frequency as highlighted in Fig. 10-a, which shows the minimum $|S_{11}|$-value in the deep centred around 135 MHz. The amplitudes of the other local minima of $|S_{11}|$, around 260 MHz and 400 MHz, have low dependence with temperature – respectively $-0.03 \cdot 10^{-3}\ \mathrm{K}^{-1}$ and $-0.15 \cdot 10^{-3}\ \mathrm{K}^{-1}$, i.e. a tenfold lower than that observed at 135 MHz. Furthermore, their resonant frequencies show a slight linear drift with temperature: the shift over the entire temperature range of interest is limited to 1.5 % and 2 % (i.e., 170 ppm · K^{-1}).

S_{21} Measurements

The system was further characterised using transmission scattering parameters, in S_{21}-shunt mode. In this configuration, ports 1 and 2 of the VNA are directly connected in parallel, together with the VNA-port of the schematic of Fig. 4.

Measured spectra are given in Fig. 9-b, showing that, similar to S_{11} measurements, there is limited dependence of the parameter with temperature, except in the frequency band cantered on the tank resonant frequency. However, as shown in Fig. 10.b, the sensitivity of $|S_{21}|$ towards temperature exhibits

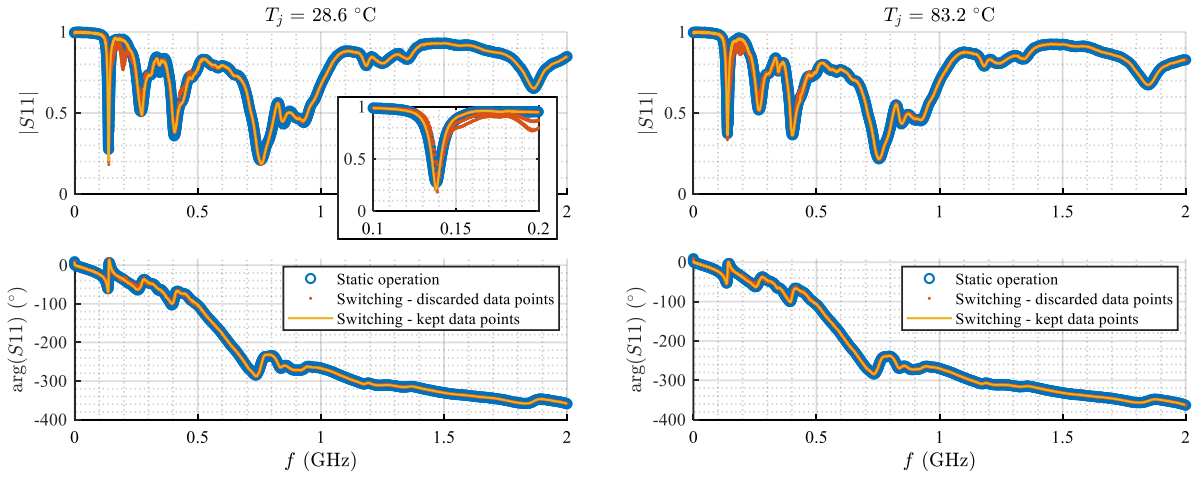

Fig. 11: Reconstruction of the spectrum of S_{11} based on measurements conducted under switching conditions, using results in static operation. At low (left) and high (right) temperature. Inset: zoom on the 135 MHz resonance.

reduced linearity and is, in average, close to half that of $|S_{11}|$.

5.2 Operation under switching conditions

Test conditions

The $R_{ds,on}$ measurements presented in the previous section were conducted online, but in static condition.

It could nonetheless be performed under switching operation by synchronising the VNA and the PWM signal, and by ensuring that the converter remains in the correct state during a complete measurement. This is realistic, given that a converter operating at 90% duty cycle at 100 kHz would leave 1 µs to perform the LS-$R_{ds,on}$ measurement – corresponding to 100 period of a 100 MHz stimuli.

However, due to non-fundamental intrinsic limitations, the used VNA requires 300 µs to perform a single measurement point (regardless the excitation frequency) and could not be synchronised with the PWM signal. Online LS-$R_{ds,on}$ measurements reported in this section were therefore conducted at a very low switching frequency and duty cycle (200 Hz and 20%, leading to $t_{on,LS} = 4$ ms) and measured data points that had not been fully measured during the on-time were discarded ex-post.

Experimental results

Fig. 11 shows the S_{11} spectrum measured in static operation (blue), the data points measured under switching condition (red), and the resulting reconstructed spectrum (yellow). In particular, the zoom around 135 MHz, in inset, shows several sets of aligned data points, or modes, corresponding to measurements performed in a specific state of the power circuit (e.g., high side transistor on or off).

The good match between the static measurements and some of the modes validates the S_{11} spectrum measurement on-line, in a switching power converter.

Discussion on the reconstruction method

The selection of relevant data point for S-parameters spectrum reconstruction was conducted assuming that the static S_{11}-spectrum was known. This would therefore render the approach unapplicable for online condition monitoring. Nonetheless, it was merely applied here to demonstrate the limited effect of switching on the measurable response. Furthermore, it would not be required, should an instrument synchronised with the PWM signal be used.

The approach could therefore be applied for in operando S_{11}-spectrum measurement.

6 Discussion

The resonant frequency of the LC-circuit was set around 135 MHz, in a frequency band where propagation effect would remain limited (wavelength close to 1 m), but high enough so that the switching noise from the GaN circuit would not significantly interfere with the measurements. High Q factors were intended in order to limit the bandwidth required by the measurement, so that the rest of the spectrum could be used for other purposes. However, the high dynamic resistance of the diode (~10 Ω) yields a relatively low Q-value, resulting in the occupation of a wide spectral band for the measurement. With future customised IC designs, a more suitable sensing device can be dimensioned.

Given the range of impedance of the dc-link, measurement of the S_{21} parameter in shunt configuration (ports 1 and 2 are directly connected in parallel with the capacitively-coupled dc-link) rather than the S_{11} would be preferable to improve accuracy [15]. Nonetheless, in the view of simplicity and to limit additional costs, most results presented in this paper focus on S_{11}.

The injection of stimulus on the DC link did not show to have an impact on the converter operation. As a matter of fact, the injected signal amplitude is only -10 dBm (i.e. 71 mV_{rms} on 50 Ω), and the attenuation from the VNA port to the LISN or the output was measured as > 8 dB up to at least 1 GHz. As a result, no electromagnetic compatibility (EMC) issue is expected.

Frequency domain measurements bring significant advantages compared to time-domain V_{ce}- or $R_{ds,on}$-based temperature measurements. In particular, noise is reduced by the intrinsic synchronous measurement, and there is no need for accurate V_{ds} and I_d measurements. On the other hand, this requires more extensive test hardware. Although a low-end VNA was demonstrated in this study to be sufficient, it would add a significant cost to the monitored circuit. This extra-cost may only be viable for mission critical and high down-time cost applications. In fact, this study is part of a larger approach intending to use microwave injection for communication and monitoring within power modules. As shown in [17], ageing has an impact on S-parameters, and temperature not only influences S_{11} around the resonator's frequency, but, to a certain extent, over the entire spectrum. A holistic method would be required to decouple and extract the effects of temperature and ageing on the response.

7 Conclusion

Knowledge of power device temperature is of high interest to implement various control strategies and expand the capabilities of power converters, especially when considering more fragile GaN devices. This paper proposed a new approach for online-estimation of the temperature of GaN HEMTs using their $R_{ds,on}$ or on-chip sensors, by measuring their resistance directly in the frequency domain using a vector network analyser (VNA). Experimental validation is demonstrated in a converter processing power. Following previous research, the approach demonstrated the potential of microwave injection for communication and monitoring within a power circuit.

References

[1] J. Kuprat, C. H. van der Broeck, M. Andresen, S. Kalker, M. Liserre, and R. W. De Doncker, "Research on Active Thermal Control: Actual Status and Future Trends," *IEEE J. Emerg. Sel. Top. Power Electron.*, vol. 9, no. 6, pp. 6494–6506, Dec. 2021, doi: 10.1109/JESTPE.2021.3067782.

[2] M. Landel, C. Gautier, and S. Lefebvre, "Study of short-circuit robustness of p-GaN and cascode transistors," *Microelectron. Reliab.*, vol. 138, p. 114695, Nov. 2022, doi: 10.1016/j.microrel.2022.114695.

[3] J. A. del Alamo and E. S. Lee, "Stability and Reliability of Lateral GaN Power Field-Effect Transistors," *IEEE Trans. Electron Devices*, vol. 66, no. 11, pp. 4578–4590, Nov. 2019, doi: 10.1109/TED.2019.2931718.

[4] S. Kalker *et al.*, "Reviewing Thermal-Monitoring Techniques for Smart Power Modules," *IEEE J. Emerg. Sel. Top. Power Electron.*, vol. 10, no. 2, pp. 1326–1341, Apr. 2022, doi: 10.1109/JESTPE.2021.3063305.

[5] S. Zhu, A. Fayyaz, and A. Castellazzi, "Static and dynamic TSEPs of SiC and GaN transistors," in *9th Int. Conf. on Power Electronics, Machines and Drives (PEMD 2018)*, Apr. 2018.

[6] L. Zhang, P. Liu, S. Guo, and A. Q. Huang, "Comparative study of temperature sensitive electrical parameters (TSEP) of Si, SiC and GaN power devices," in *2016 IEEE 4th Workshop on Wide Bandgap Power Devices and Applications (WiPDA)*, Nov. 2016, pp. 302–307. doi: 10.1109/WiPDA.2016.7799957.

[7] S. Kalker, C. Van der Broeck, L. Ruppert, and R. De Doncker, "Next Generation Monitoring of SiC MOSFETs via Spectral Electroluminescence Sensing," *IEEE Trans. Ind. Appl.*, vol. Early Access, Mar. 2021, doi: 10.1109/TIA.2021.3062773.

[8] N. Baker, M. Liserre, L. Dupont, and Y. Avenas, "Junction temperature measurements via thermo-sensitive electrical parameters and their application to condition monitoring and active thermal control of power converters," in *IECON 2013 - 39th Annual Conf. IEEE Ind. Electronics Society*, Nov. 2013, pp. 942–948. doi: 10.1109/IECON.2013.6699260.

[9] N. Baker, F. Iannuzzo, S. Munk-Nielsen, L. Dupont, and Y. Avenas, "Experimental Evaluation of IGBT Junction Temperature Measurement via a Modified-VCE (ΔVCE_ΔVGE) Method with Series Resistance Removal," in *Int. Conf. on Integrated Power Electronics Systems (CIPS)*, Mar. 2016, pp. 1–6.

[10] S. Moench *et al.*, "A 600V p-GaN Gate HEMT with Intrinsic Freewheeling Schottky-Diode in a GaN Power IC with Bootstrapped Driver and Sensors," in *Int. Symp. on Power Semiconductor Devices and ICs (ISPSD)*, Sep. 2020, pp. 254–257. doi: 10.1109/ISPSD46842.2020.9170089.

[11] M. Basler, R. Reiner, S. Moench, P. Waltereit, R. Quay, and J. Haarer, "Compact GaN Power ICs with Power HEMT, Gate Driver, Temperature Sensor, Current Sense-FET and Amplifier," in *IEEE 35th IEEE Int. Symp. on Power Semiconductor Devices and ICs (ISPSD)*, 2023.

[12] R. Reiner *et al.*, "Linear temperature sensors in high-voltage GaN-HEMT power devices," in *2016 IEEE Applied Power Electronics Conference and Exposition (APEC)*, Mar. 2016, pp. 2083–2086. doi: 10.1109/APEC.2016.7468154.

[13] D. Reusch and J. Strydom, "Understanding the Effect of PCB Layout on Circuit Performance in a High-Frequency Gallium-Nitride-Based Point of Load Converter," *IEEE Trans. Power Electron.*, vol. 29, no. 4, pp. 2008–2015, Apr. 2014, doi: 10.1109/TPEL.2013.2266103.

[14] Y. Pascal, D. Labrousse, M. Petit, and F. Costa, "Study of the Impedance of the Bypassing Network of a Switching Cell – Influence of the Positioning of the Decoupling Capacitors," in *2019 IEEE International Workshop on Integrated Power Packaging (IWIPP)*, Apr. 2019, pp. 120–124. doi: 10.1109/IWIPP.2019.8799093.

[15] "Impedance Measurement Handbook ed. 6 | Keysight." 2016.

[16] "NanoVNA V2 (S-A-A-2). NanoVNA V2." https://github.com/nanovna-v2/NanoVNA2

[17] Y. Pascal, F. Daschner, M. Liserre, and M. Höft, "Condition monitoring of power module using S-parameters, TDR, and TDT," *Microelectron. Reliab.*, vol. 138, p. 114615, Nov. 2022, doi: 10.1016/j.microrel.2022.114615.